J. Wind Eng. Ind. Aerodyn. 146 (2015) 39–50

Contents lists available at ScienceDirect

Journal of Wind Engineering and Industrial Aerodynamics

journal homepage: www.elsevier.com/locate/jweia

A study of tornado induced mean aerodynamic forces on a gable-roofed building by the large eddy simulations

Zhenqing Liu [a,*], Takeshi Ishihara [b]

[a] School of Civil Engineering and Mechanics, Huazhong University of Science and Technology, Wuhan, Hubei, China
[b] Department of Civil Engineering, School of Engineering, The University of Tokyo, Tokyo, Japan

ARTICLE INFO

Article history:
Received 13 March 2015
Received in revised form
10 August 2015
Accepted 10 August 2015

Keywords:
Tornado-like vortex
Building model
Aerodynamic forces
Force coefficients
LES

ABSTRACT

A tornado simulator was built and tornado-induced mean aerodynamic forces on a gable-roofed building were numerically studied. Simulated mean flow fields and mean forces acting on a building model showed satisfactory agreement with those from experiments verifying the accuracy of the tornado simulator. Around the world experimental tornado simulators are very limited which makes estimating tornado induced forces much difficult. Therefore, examining whether or not there are any relationships between tornado induced forces and straight-line wind induced forces is the target of this study. After checking mean wind profiles below the height of building in tornado flow fields, a kind of spiral was found. This spiral is unique compared with profiles in traditional wind tunnel. Therefore a concept of volume averaged velocity was proposed and found to be the linkage between tornado induced mean forces and straight-line wind induced mean forces, i.e. removing tornado induced atmospheric pressures, the building in tornado experiences similar responses with those in wind tunnel if the direction of volume averaged velocity is same. Based on this finding, a method estimating the tornado-induced mean aerodynamic forces using the straight-line wind tunnel is proposed and the results transformed from the data base of the straight-line wind tunnel show satisfactory agreement with those directly calculated in the tornado simulator.

© 2015 Elsevier Ltd. All rights reserved.

1. Introduction

Straight-line wind induced aerodynamic forces have been extensively studied in past decades experimentally and numerically [see, e.g. Hoxey and Richards (1993), Mochida et al. (1993), Tamura et al. (1997, 2001, 2008), Kopp and Chen (2006), Blocken et al. (2007), and Yang et al. (2008)]. Tornado-induced forces are not studied as extensively as those by the straight-line wind. Tornadoes are among the most violent storms occurring in the atmospheric boundary layer. Thousands of tornadoes are reported every year and they cause incredible amounts of damage as well as significant numbers of fatalities, e.g. in 2011, more than 1000 tornadoes occurred in the U.S., due to which at least 550 people were perished, as reported by Doswell et al. (2012). Therefore it is important to take proper consideration of tornado-induced wind loads and tornado-borne debris for wind resistant design of structures. More and more attentions were paid to reveal the complicated flow structures [see, e.g., Ward (1972), Church et al. (1979), Monji (1985), Lee and Wilhelmson (1997a, 1997b), Lewellen et al. (2000), Hangan and Kim (2008), Matsui and Tamura (2009), Tari et al. (2010), Ishihara et al. (2011), and Maruyama (2011)]. With the improvement of understanding about tornado-like flow fields, estimation of tornado-induced aerodynamic forces on structures is now becoming a new goal.

Considering the difficulty of observing tornados in nature, laboratory simulations are now the main approach for studying the tornado-induced aerodynamic forces and three types of tornado simulators are used. The first type is the Ward-type simulator developed by Ward (1972) which could only be used to study the stationary tornado. Jischke and Light (1983) applied the Ward-type simulator to study the interaction between tornado flow fields and structures and proposed that an addition of swirl to the flow significantly changes the forces acting on the model. Mishra et al. (2008) also applied Ward-type simulator to generate a single-celled tornado-like vortex and studied the wind loading on a cubical model. It was found that the pressure distributions and forces exhibit quite different characteristics in comparison with those from wind tunnel. Rajasekharan et al. (2013a) performed an experimental investigation using the tornado simulator at Tokyo Polytechnic University which is also a Ward type simulator and obtained a better understanding of the effects of building location with respect to vortex. Rajasekharan et al. (2013b) then analyzed

* Corresponding author.
E-mail address: liuzhenqing1984@hotmail.com (Z. Liu).

http://dx.doi.org/10.1016/j.jweia.2015.08.002
0167-6105/© 2015 Elsevier Ltd. All rights reserved.

Nomenclature

$C_{F_{it},v_{H,max}}$	total force normalized by $v_{H,max}$
$C_{F_{ip},v_{H,max}}$	force due to pressure drop normalized by $v_{H,max}$
$C_{F_{iw},v_{H,max}}$	force due to direct impact of wind normalized by $v_{H,max}$
C_{F_{iw},V_H}	force due to direct impact of wind normalized by V_H
C_{F_{iw},V_v}	force due to direct impact of wind normalized by V_V
$C_{F_{i,e.b.}}$	force due to direct impact of wind at the end bay region normalized by V_H
d	diameter of the updraft hole
F_{ip}	forces associated with the tornado-induced pressure drop
F_{iw}	forces caused by the direct impact of wind upon the structure
F_{im}	impactive forces caused by tornado-borne missiles
$F_{i,e.b.}$	time averaged aerodynamic forces at the end bay region
h	height of the inlet layer
Q	flow rate
r_c	radius at which v_c occurs
$r_{H,max}$	radius at which $v_{H,max}$ occurs
Re_b	reynolds number for the building model
Re_t	tornado reynolds number
V_T	translating speed
V_v	volume averaged wind speed
V_H	wind speed at m.e.h.
v_c	maximum tangential velocity in the quasi-cylindrical region
v_{xH}	time-averaged radial velocity
v_{yH}	time-averaged tangential velocity
v_{zH}	vertical velocity at m.e.h.
$v_{H,max}$	maximum tangential velocity, at m.e.h.
λ_L	tornado size scale
λ_{vel}	velocity scale
λ_B	ratio of the building size to the size of the tornado
θ_H	angle of attack at m.e.h.
θ_S	angle of attack at surface
θ_v	volume averaged angle of attack
Ω	volume occupied by the building model
m.e.h.	mean eave height
e.b.	end bay region

the effect of ground roughness on the internal pressures developed inside a building model exposed to a stationary vortex. The second type is the tornado simulator developed in Iowa State University (ISU) which could simulate both stationary and translating tornadoes. The details of this type of simulator have been introduced in Haan et al. (2008). Haan et al. (2010) then presented transient wind loads on a one-story, gable-roofed building in a laboratory-simulated tornado and showed that the tornado-induced lateral forces were about 50% larger than those by ASCE 7-05 and uplift forces in tornado were two or three times as large as those by the provision. Yang et al. (2010, 2011) experimentally quantified the characteristics of the wind loads on a gable-roofed building and a high-rise building using the ISU tornado simulator, from which the significant difference between tornado induced forces and straight-line wind induced forces was discussed. The last one is the torando simulator developed in WindEEE (Wind Engineering, Energy and Environment Research Institute) Dome at Western University as reported by Refan (2014). However, the tornado simulators around the world are limited, therefore it is meaningful to propose a method estimating tornado-induced forces by the wind tunnel.

There are very few numerical researches associated with tornado-induced forces so far. Wilson (1977) firstly applied a two dimensional numerical model to examine the effects of tornadoes on buildings, in which only horizontal forces were calculated. However, flow fields in tornado are three dimensional and the lift force regarded as an important factor causing the damage of buildings could not be calculated by this two-dimensional numerical simulator. Alrasheedi and Selvam (2011) applied a three-dimensional model to compare the wind loads from tornado and those from straight-line winds. They concluded that it is not sufficient to estimate the wind loads using wind tunnels; however, tornado-like flow fields in their study were provided from a Rankine combined vortex model. Therefore, a three-dimensional numerical simulation about the tornado-induced aerodynamic forces on buildings with flow fields directly generated from a three-dimensional numerical tornado simulator is needed to be carried out.

In this study, tornado-induced mean forces acting on a gable-roofed building are calculated numerically by large eddy simulations in a three-dimensional model and a method estimating tornado-induced mean forces by aerodynamic coefficients from wind tunnels is proposed. In Section 2, the setups of a numerical tornado simulator and a numerical wind tunnel are introduced. Accuracies of the numerical tornado simulator and the numerical wind tunnel are validated in Section 3, where the flow fields as well as the mean forces acting on a building model are investigated. In Section 4, a method evaluating the tornado-induced forces on the building through the straight-line wind tunnel is proposed.

2. Numerical models

In this section, the governing equations and the solution scheme are firstly outlined, followed by the introduction of the gable-roofed building model. Then the setups for the numerical tornado simulator and the numerical wind tunnel are introduced, including its geometry, mesh and boundary conditions.

2.1. Governing equations and solution schemes

In this study, large eddy simulation (LES) is adopted, in which large eddies are computed directly, while the influence of eddies smaller than grid spacing is modeled. Boussinesq hypothesis is employed and standard Smagorinsky–Lilly model is used to calculate the subgrid-scale (SGS) stresses.

The governing equations applied in LES model are obtained by filtering the time-dependent Navier–Stokes equations in Cartesian coordinates (x, y, z) and expressed in the form of tensor as follows:

$$\frac{\partial \rho \tilde{u}_i}{\partial x_i} = 0 \tag{1}$$

$$\frac{\partial \rho \tilde{u}_i}{\partial t} + \frac{\partial \rho \tilde{u}_i \tilde{u}_j}{\partial x_j} = \frac{\partial}{\partial x_j}\left(\mu \frac{\partial \tilde{u}_i}{\partial x_j}\right) - \frac{\partial \tilde{p}}{\partial x_i} - \frac{\partial \tau_{ij}}{\partial x_j} \tag{2}$$

where $\tilde{u}_i$ and $\tilde{p}$ are the filtered velocities and pressure, respectively, μ is the viscosity, ρ is the density, τ_{ij} is the SGS stress, which is modeled as follows:

$$\tau_{ij} = -2\mu_t \tilde{S}_{ij} + \frac{1}{3}\tau_{kk}\delta_{ij}, \quad \tilde{S}_{ij} = \frac{1}{2}\left(\frac{\partial \tilde{u}_i}{\partial x_j} + \frac{\partial \tilde{u}_j}{\partial x_i}\right) \tag{3}$$

where μ_t denotes the SGS turbulent viscosity, $\tilde{S}_{ij}$ is the rate-of-strain tensor for the resolved scale, and δ_{ij} is the Kronecker delta. The Smagorinsky–Lilly model is used for the SGS turbulent viscosity

$$\mu_t = \rho L_s^2 \left|\tilde{S}\right| = \rho L_s \sqrt{2\tilde{S}_{ij}\tilde{S}_{ij}};\ L_s = \min(\kappa d, C_s V^{1/3}) \tag{4}$$

in which L_s denotes the mixing length for subgrid-scales, κ is the von Kármán constant, i.e., 0.42, d is the distance to the closest wall and V is the volume of a computational cell. In this study, C_s is Smagorinsky constant, which is determined to be 0.032 based on Oka and Ishihara (2009).

For the wall-adjacent cells, when they are in the laminar sublayer, the wall shear stresses are obtained from the laminar stress–strain relationship

$$\frac{\tilde{u}}{u_\tau} = \frac{\rho u_\tau y}{\mu} \tag{5}$$

If the mesh cannot resolve the laminar sublayer, it is assumed that the centroid of the wall-adjacent cells falls within the logarithmic region of the boundary layer, and the law-of-the-wall is employed, which is expressed as

$$\frac{\tilde{u}}{u_\tau} = \frac{1}{\kappa}\ln E\left(\frac{\rho u_\tau y}{\mu}\right) \tag{6}$$

where $\tilde{u}$ is the filtered velocity tangential to wall, y is the distance between the center of the cell and the wall, u_τ is the friction velocity, and the constant E is 9.793.

Finite volume method is used for the present simulations. The second order central difference scheme is used for the convective and viscosity term, and the second order implicit scheme for the unsteady term. SIMPLE (semi-implicit pressure linked equations) algorithm is employed for solving the discretized equations (Ferziger and Peric, 2002).

2.2. Gable-roofed building model

A gable-roofed building model with a 24 m × 38 m plan, height of 12.2 m and roof slope of 1:12 in full scale, same as those in the experiment by Kikitsu et al. (2012) who studied the aerodynamic forces acting on the building by an ISU tornado simulator which was developed in Building Research Institute (BRI), Japan, and those by Pierre et al. (2005) who studied the aerodynamic forces on the building by the traditional straight-line wind tunnel, is chosen in the present study. The length scale of the simulated tornado is 1:1900 by matching the size of numerical tornado with a real tornado, as discussed in the following subsection, thus this scale is also applied for the building model. The scaled dimension and the orientation of the building are illustrated in Fig. 1(a), where L, D and H are the length, width and mean eave height, m.e.h., of the building model, respectively, and θ indicates the angle of attack. The red region in Fig. 1(a) illustrates an end bay region which will be used to verify the accuracy of the numerical wind tunnel by comparing the mean forces on these surfaces with those in the experiments by Pierre et al. (2005). In the experiment by Kikitsu et al. (2012) and that by Pierre et al. (2005), the surfaces of the building model were smooth, therefore the wall boundary condition without any roughness is used at the surfaces of the building. Details of the grid distribution on surfaces of the building are shown in Fig. 1(b). Small size meshes were generated near each edge corner to capture the complicate turbulent flow fields here, and 40 meshes were used in width, length, and height directions. The grid distributions on the surfaces of building model will be applied in both the numerical tornado simulator and numerical wind tunnel. Table 1 illustrates the parameters for this gable-roofed building model and those in the experiments.

2.3. Numerical tornado simulator

The configurations of the numerical tornado simulator, which is the Ward type tornado simulator and identical with that in the study by Ishihara and Liu (2014), are shown in Fig. 2(a). Two significant geometry parameters are the height of the inlet layer, h, and the radius of the updraft hole, r_0, which are 200 mm and 150 mm respectively. Fig. 2(b) shows the mesh system of the numerical tornado simulator. In order to accurately capture the flow fields of tornado-like vortices and quantitatively investigate the wind loading on the building, in the central part of convergent zone and the vicinity near the ground, a fine mesh is considered. The minimum grid size is 0.15 mm in both vertical and horizontal directions. The growing ratios in the two directions are less than

Table 1
Parameters of test building model and those in experiments.

	Present simulation	Exp. by Kikitsu	Exp. by Pierre
Mean eave height of building model: H	6.4 mm	35 mm	122 mm
Length of building model: L	20 mm	109 mm	380 mm
Width of building model: D	13 mm	70 mm	240 mm
Slope of the roof	1:12	1:12	1:12
Length scale: λ_L	1:1900	1:350	1:100
Mesh size in the height direction	0.15 mm	\	\
Mesh size in the length direction	0.15–0.5 mm	\	\
Mesh size in the width direction	0.15–0.2 mm	\	\

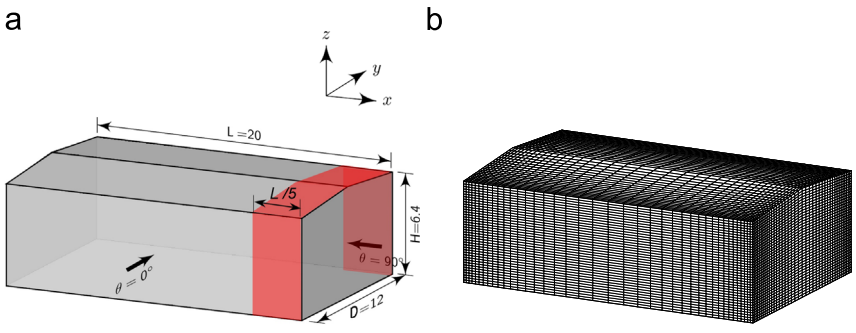

Fig. 1. Building model, (a) geometry and (b) grid (mm) (For interpretation of the references to color in this figure legend, the reader is referred to the web version of this article).

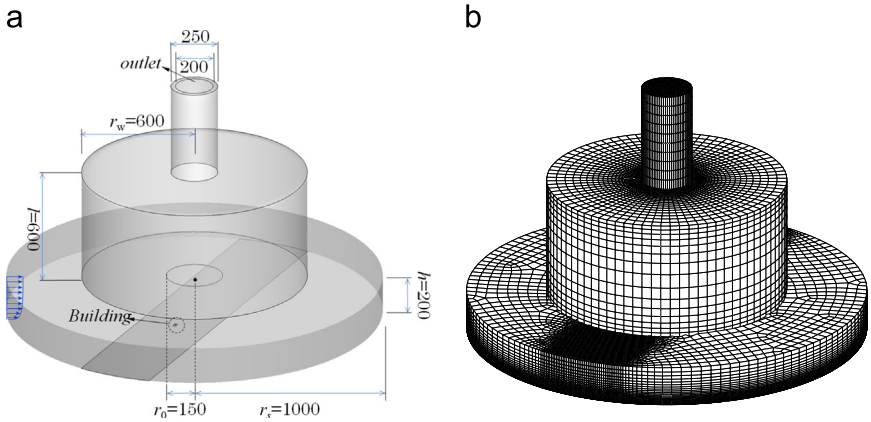

Fig. 2. Numerical tornado simulator, (a) geometry and (b) grid system (mm).

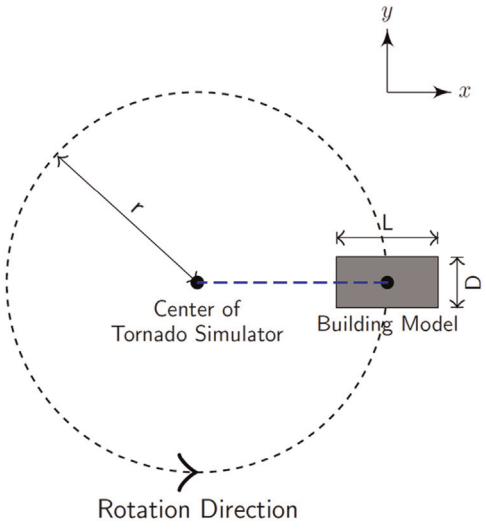

Fig. 3. Relative location between tornado and building.

1.2 in order to avoid a sudden change of the grid size. The total mesh number is about 8×10^5. The relative location between the building model and tornado is illustrated in Fig. 3, where r indicates the distance between them.

In order to get the time averaged forces on the building, same as the study by Yang et al. (2011), the building was tested in a stationary tornado with 13 different distances to the center of tornado, from 0 mm to 240 mm with a step size of 20 mm. At each location the time averaged aerodynamic forces were obtained by running the simulation for 30 s and the first 10 s data were removed to eliminate the transient results. The wind profile at the inlet are specified as

$$\begin{cases} u_{r_s} = u_1 (z/z_1)^{1/n} \\ u_{r_s} = -u_{r_s} \tan(\phi) \end{cases} \tag{7}$$

where u_{r_s} and v_{r_s} are radial and tangential velocities at $r = r_s$, n equals to 7.0, the reference velocity u_1 and the reference height z_1 are set to 0.24 m/s and 0.01 m respectively, ϕ is the inflow angle specified as 84.4°, the tornado size scale, λ_L, and velocity scale, λ_{vel}, were found to be 1:1900 and 1:3.05 respectively by comparing the flow fields with those in the Spencer F4 tornado, occurring in Spencer, South Dakota, the US in 1998, observed by Wurman and Alexander (2005). The method determining the scale of simulated tornado could be found in the study by Hangan and Kim (2008).

Table 2
Parameters for numerical tornado simulator and those in experiment.

	Present simulation	Exp. by Kikitsu
Height of the inlet layer: h	200 mm	\
Radius of the updraft hole: r_0	150 mm	\
Internal aspect ratio: $a = h/r_0$	1.33	\
Radius of the exhaust outlet: r_t	100 mm	\
Radius of the convergence region: r_s	1000 mm	\
Velocity at the outlet: w_0	9.55 m/s	\
Total outflow rate: $Q = \pi r_t^2 w_0$	0.3 m^3/s	\
Inflow angle: ϕ	88.4°	\
Non-dimensional time step: $\Delta t v_{H,\,max}/L$	0.04	\
Maximum tangential velocity at m.e.h: $v_{H,\,max}$	22.8 m/s	9.8 m/s
Radius at which $v_{H,\,max}$ occurs: $r_{H,\,max}$	0.06 m	0.12 m
Maximum tangential velocity at high level: v_c	18.6 m/s	\
Radius at which v_c occurs: r_c	0.112 m	\
Translation speed: V_T	\	0.06 m/s
Swirl ratio: S	2.44	\
Building Reynolds number: $Re_b = v_{H,\,max} L/\nu$	2.50×10^4	5.80×10^4
Tornado Reynolds number: $Re_t = w_0 d/\nu$	1.60×10^5	\
Mesh size in the radial direction	0.15–25.0 mm	\
Mesh size in the vertical direction	0.15–5.0 mm	\
Mesh number	8×10^5	\

Outflow condition was specified at the outlet of the simulator with gradients of the velocities and the pressure set to be 0.

Reynolds number for the building model, $Re_b = v_{H,\,max} L/\nu$, where $v_{H,\,max}$ is the maximum tangential velocity, 22.8 m/s, at m.e.h., is calculated as 2.50×10^4. Reynolds number of the tornado, $Re_t = w_0 d/\nu$, is calculated as 1.6×10^5, where w_0 is the updraft wind velocity at the outlet, 9.55 m/s, and d is the diameter of the updraft hole. The swirl ratio is defined as

$$S \equiv \frac{\pi r_c^2 v_c}{Q} \tag{8}$$

where r_c is radius at which the maximum tangential velocity, v_c, in the quasi-cylindrical region occurs, and Q is the flow rate, following the definition by Haan et al. (2008). The parameters r_c, v_c and Q are measured as 0.112 m, 18.6 m/s and 0.3 m^3/s, respectively, therefore the swirl ratio is 2.44. The radius, $r_{H,\,max}$, at which $v_{H,\,max}$ occurs, is measured as 0.06 m. Table 2 illustrates the parameters for the tornado simulator and those in the experiment by Kikitsu et al. (2012).

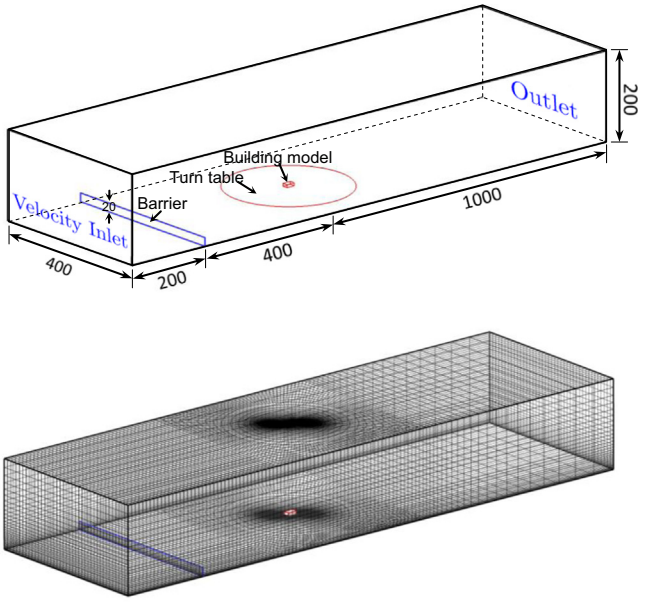

Fig. 4. Geometry (a) and grid system (b) for numerical wind tunnel (mm).

Table 3
Parameters for numerical wind tunnel and those in the experiment.

	Present simulation	Exp. by Pierre
Height of computation domain	200 mm	\
Length of computation domain	1200 mm	\
Width of computation domain	400 mm	\
Wind speed at m.e.h.: V_H	22.8 m/s	8.7 m/s
Building Reynolds number: $Re_b = V_H L/\nu$	2.50×10^4	1.81×10^5
Non-dimensional time step: $\Delta t V_H/L$	0.04	\
Mesh size in the radial direction	0.15–25.0 mm	\
Mesh size in the vertical direction	0.15–5.0 mm	\
Mesh number	3×10^5	\

2.4. Numerical wind tunnel

The numerical wind tunnel is shown in Fig. 4(a). The height of the numerical wind tunnel is same with that of convergence region in numerical tornado simulator which is 200 mm. The width and length of the numerical wind tunnel are 400 mm and 1200 mm respectively. The building model was mounted at the center of turntable which is used to specify the angle of attack, θ. The distance between the center of turntable and a barrier is 400 mm. 20 mm is chosen for the height of the barrier to generate proper boundary layer flows. The distance from the inlet to the barrier is 200 mm. A structured grid is used with a coarse mesh near the outlet and a fine mesh in the vicinity surrounding the building model, as shown in Fig. 4(b). The minimum grid size in both vertical and horizontal directions, and the grid growing ratio near the building are same with those used in the tornado simulator, with an attempt to remove the influence from gird differences. Total mesh number is about 8.0×10^5. The building model was placed at the center of turntable.

At the inlet an uniform wind speed, 35.2 m/s, is provided. Due to the disturbance from the barrier, at the location where the building mounted the wind speed at m.e.h., V_H decreases to 22.8 m/s which is same as $v_{H,\,max}$ in the simulated tornado, making the Reynolds number for the building model in these two situations identical. The outflow condition was specified at the outlet. Table 3 illustrates the computational parameters for the numerical wind tunnel and those in the experiment by Pierre et al. (2005). The building model was tested with five different angles of attack, θ (10°, 20°, 30°, 40°, and 50°). At each angle of attack the time averaged aerodynamic forces were obtained by running the simulation for 30 s and the first 10 s data were removed to eliminate transient results.

3. Numerical results and validations

In almost all of experiments about the tornado induced forces (Jischke and Light, 1983; Mishra, et al., 2008; Yang et al., 2011; Hu et al., 2011), they only consider the time averaged forces. The peak loadings of the tornado induced forces are very important for the wind resistant design of building, but at the current situation it is very difficult for us to consider this, because the sizes of tornado simulators are much small compared with real tornadoes as a result the Reynolds number is quite different. Therefore, same as previous researchers, we only focus on the time averaged forces. Peak loadings could be the target of future researches.

3.1. Definition of force coefficients

Rotz et al. (1974) divided the tornado-induced mean forces on structure into three parts, i.e. 1) forces associated with the tornado-induced pressure drop, F_{ip}; 2) forces caused by the direct action of air flow upon the structure, F_{iw}; 3) impactive forces caused by tornado-borne missiles, F_{im}. In the present study F_{im} is not considered. Therefore the total force, F_{it}, could be expressed as

$$F_{it} = F_{ip} + F_{iw} \tag{9}$$

where the subscript 'i' denotes x, y and z directions. In the previous studies about tornado induced forces [see Mishra et al. (2008), Haan et al. (2010), Yang et al. (2011), Kikitsu et al. (2012)]. the force coefficients are formulated as

$$C_{F_{it},v_{H,\,max}}(r) = \frac{F_{it}}{1/2\rho v_{H,\,max}^2 A_i},\quad C_{F_{ip},v_{H,\,max}}(r) = \frac{F_{ip}}{1/2\rho v_{H,\,max}^2 A_i},$$
$$C_{F_{iw},v_{H,\,max}}(r) = \frac{F_{iw}}{1/2\rho v_{H,\,max}^2 A_i} \tag{10}$$

in which the force coefficients are the function of the radial location, r, in tornado, $v_{H,\,\max}$ is the maximum tangential velocity at the mean eave height of building, A_i denotes the projection area in x, y and z directions, $A_x = DH$, $A_y = HL$, and $A_z = DL$.

In the wind tunnel, there is no force due to the pressure drop, therefore the total forces, F_{it}, are only caused by the direct action of air flow upon the structure. In the previous study about the wind induced forces on buildings, see Pierre et al. (2005), the force coefficients are formulated as

$$C_{F_{iw},V_H}(\theta) = \frac{F_{iw}}{1/2\rho V_H^2 A_i} \tag{11}$$

in which the force coefficients are the function of the angle of attack, θ. V_H is the wind speed at the mean eave height of the building.

3.2. Numerical results and validations for the tornado simulator

Same as the experiment by Kikitsu et al. (2012), the numerical simulator was firstly run with the absence of the building to get the time averaged flow fields of a stationary tornado. The time-averaged radial velocity, v_{xH}, whose positive direction is outward the center of the simulator, tangential velocity, v_{yH}, and vertical velocity, v_{zH}, at m.e.h., were normalized by the constant speed $v_{H,\,max}$ and the results of time averaged tangential velocity show good agreement with those in the study by Kikitsu et al. (2012).

The maximum difference between the numerical results and the experimental results is only 15% occuring at the location of $r=0.4r_{H,max}$. Tornado-induced pressure drop on the ground normalized by $v_{H,max}$ is illustrated in Fig. 5(b), where a great pressure drop can be clearly found at the center of tornado. Therefore, it can be imagined that at the center the vertical force acting on the gable-roof building is very large, which is the explanation why the buildings destroyed by tornados are always observed to be with roofs lifted off. Superimposed on Fig. 5(b) is the data in the study by Kikitsu et al. (2012) and the comparison between the numerical and experimental results shows differences within the range of 10%.

In the experimental study by Kikitsu et al. (2012), the simulator was then translated at a speed $V_T=0.06$ m/s and the transient forces were measured. The ratio of the translating speed to the maximum tangential speed at m.e.h., $v_{H,max}$, is only 0.6% which is too small and the effects from the translation of the tornado could be neglected. In the following validation, we will directly do the comparison between the stationary tornado induced time averaged aerodynamic forces in the present study with the ensemble averaged ones in the experiments by Kikitsu et al. (2012) which are the average of 10 runs.

Fig. 6(a) shows the time averaged total force coefficients, $C_{F_{it},v_{H,max}}$, on the building at several radial locations in the tornado. The tornado-induced force in x direction, $C_{F_{xt},v_{H,max}}$, is negative and the magnitude of it increases from 0 at the center to maximum at $r=1.3r_{H,max}$ followed by a gentle decrease. The tornado-induced force in y direction, $C_{F_{yt},v_{H,max}}$, shows the positive sign, implying that the building model is pushed clockwise. The lift force is different with the horizontal force components and exhibits large values at $r=0.0$ where the wind speed is zero indicating that the tornado-induced pressure drop is the sole source of large lift force here. Superimposed on Fig. 6(a) are the ensemble averaged forces from the experiment by Kikitsu et al. (2012) with largest discrepancy from the numerical results of about 10%, 12% and 25% for the forces in x, y, and z directions respectively.

$C_{F_{ip},v_{H,max}}$ are determined from Fig. 5(b) and the values are shown in Fig. 6(b). $C_{F_{xp},v_{H,max}}$ shows negative sign which means pushing the building closing to the center of tornado. This is due to the difference of the tornado induced pressure drop on the side walls. $C_{F_{yp},v_{H,max}}$ is zero due to the symmetry of the flow fields and that the building is just located at the x axis. The tornado-induced pressure drop has the effect lifting the building and $C_{F_{zp},v_{H,max}}$ shows the maximum, 2.0, at the center.

The forces coefficients due to the direct action of wind, $C_{F_{iw},v_{H,max}}$, could be obtained by removing $C_{F_{ip},v_{H,max}}$ from $C_{F_{it},v_{H,max}}$ and are shown in Fig. 6(c). It is clear that the magnitudes of all components of $C_{F_{iw},v_{H,max}}$ have the same trend with the wind speed, showing zero at the center and maximum at about $r=r_{H,max}$.

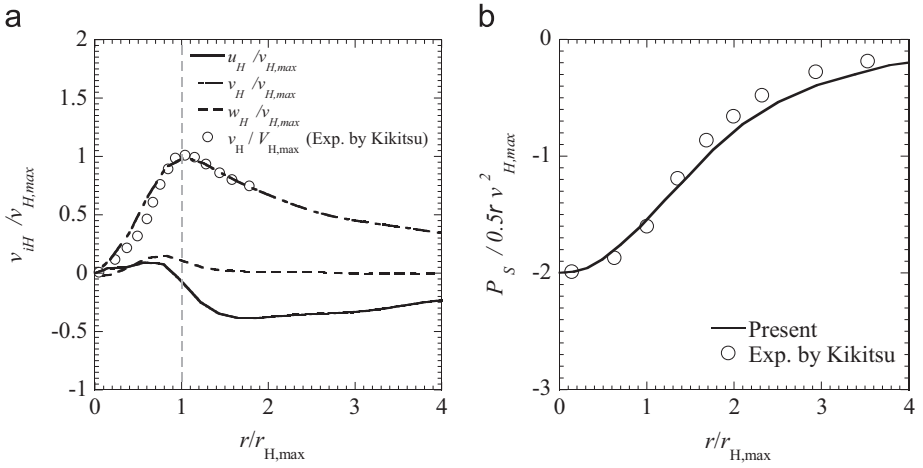

Fig. 5. Flow fields in the simulated tornado with absence of building. (a) Profiles of velocity components at mean eave height, and (b) pressure coefficient on the ground of simulator.

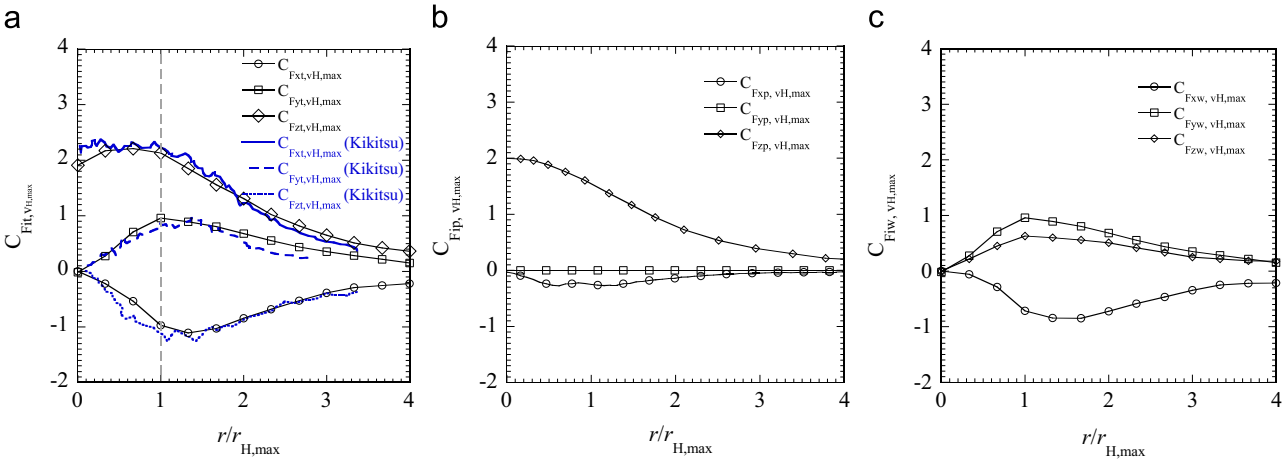

Fig. 6. Radial distribution of the force coefficients, (a) $C_{F_{it},v_{H,max}}$, (b) $C_{F_{ip},v_{H,max}}$, and (c) $C_{F_{iw},v_{H,max}}$, from numerical tornado simulator.

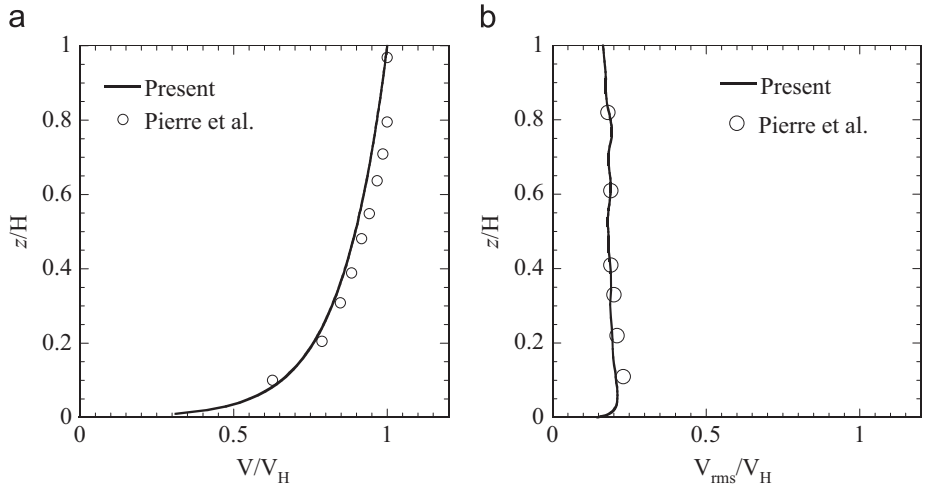

Fig. 7. Comparison of (a) normalized wind speed and (b) turbulence intensity.

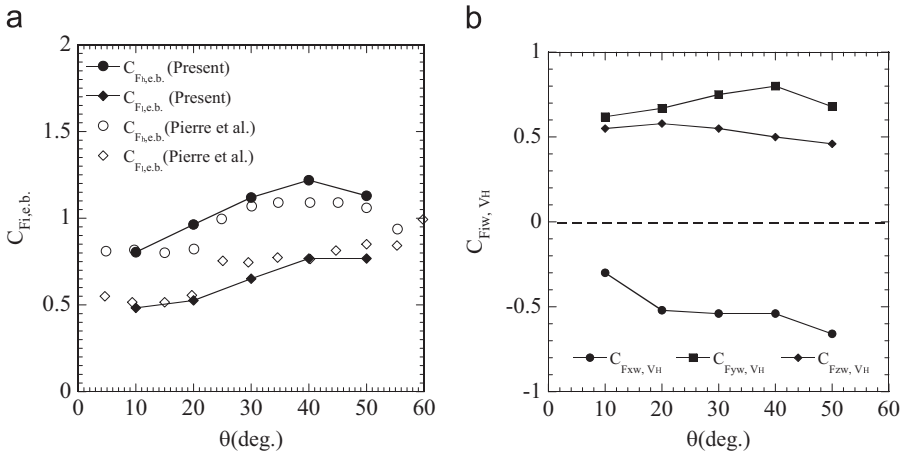

Fig. 8. Force coefficients at the end bay region, $C_{F_{i,e.b.}}$, and the whole building model, C_{F_{iw},V_H}, from the numerical wind tunnel.

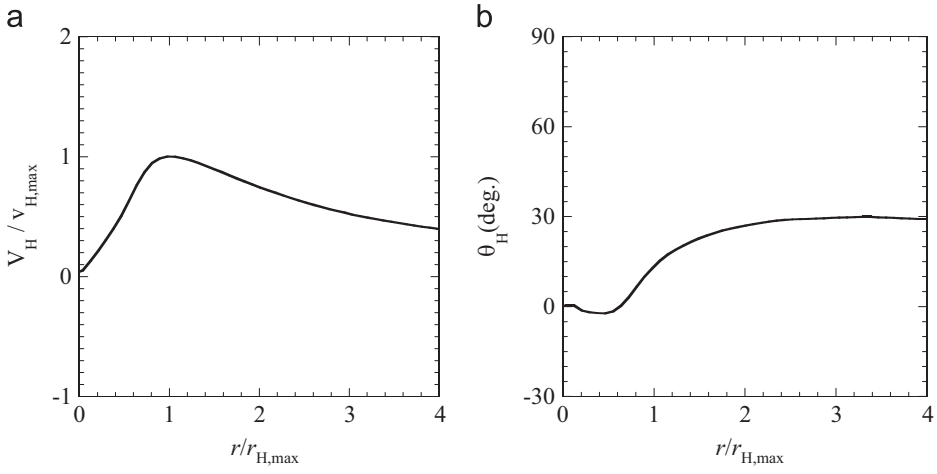

Fig. 9. Radial profiles of (a) normalized wind speed and (b) direction at mean eave height.

3.3. Numerical results and validations for the wind tunnel

The numerical results of the mean forces on the end bay region, as shown in Fig. 1(a), in the numerical wind tunnel are compared with those in the experiment by Pierre et al. (2005). The normalized mean wind speed by V_H as well as the turbulence intensity, V_{rms}/V_H, at the location where the building model is mounted is shown in Fig. 7. The mean wind speed profile and the turbulence intensity in the numerical wind tunnel give almost the same values with those in the experiment which makes sure the

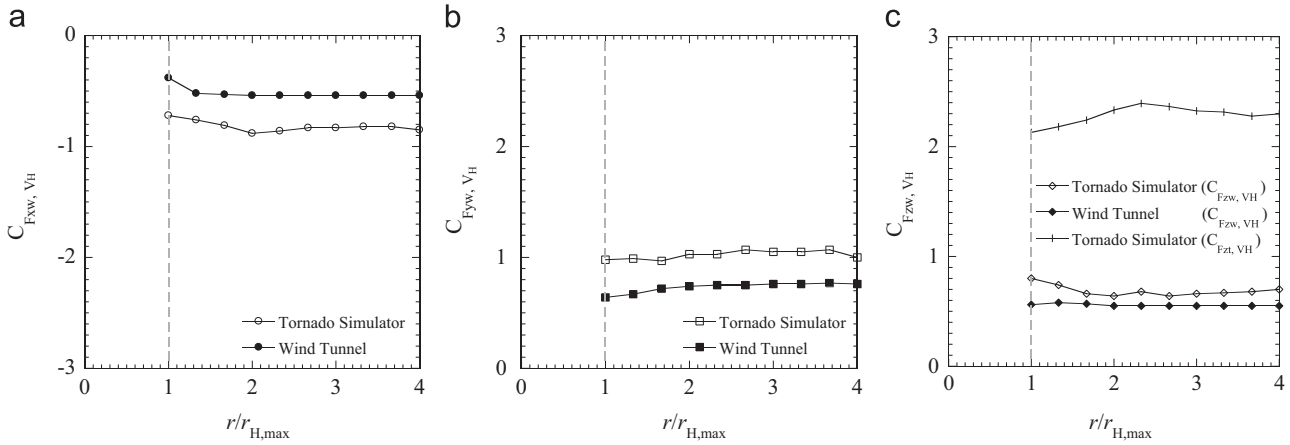

Fig. 10. Comparison of force coefficients, C_{F_{iw},V_H}, from tornado simulator and those from wind tunnel, (a) radial component, (b) tangential component, and (c) vertical component.

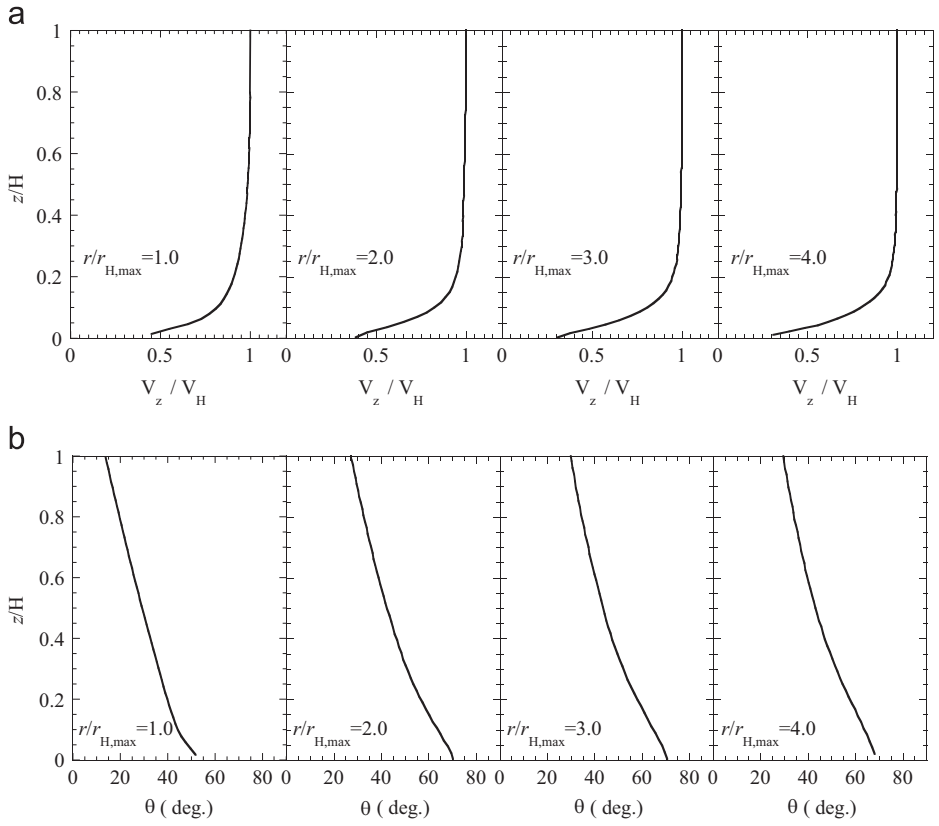

Fig. 11. Vertical profiles of (a) normalized wind speed and (b) direction at several radial locations.

following validation of aerodynamic forces meaningful. The aerodynamic force coefficient, $C_{F_{i,e.b.}}$, at the end bay region is defined as

$$C_{F_{i,e.b.}}(\theta) \equiv \frac{F_{i,e.b.}}{1/2V_H^2 A_{i,e.b.}} \tag{12}$$

in which $F_{i,e.b.}$, are the time averaged aerodynamic forces, the subscript 'i' denotes horizontal thrust, 'h', and uplift components, 'l', respectively, and $A_{h,e.b.} = LH/5$, $A_{l,e.b.} = DL/5$. The simulated forces on the same end bay region are extracted and illustrated in Fig. 8. The comparison between the simulated results and the experimental ones shows discrepancies within a range of only 10% validating the accuracy of simulated data. The force coefficients of the whole building, C_{F_{iw},V_H}, defined by Eq. (11), at five angles of attack, θ, are shown in Fig. 8 and will be used in the next section. The values in between these five angles of attack will be obtained by linear interpolation.

4. A method estimating tornado induced forces by the wind tunnel

In this section, a method is proposed to estimate tornado-induced forces using the force coefficients obtained from the wind tunnel test. The volume averaged wind speed and the volume averaged angle of attack are proposed to deal with these two different situations.

The comparison between the force coefficients, C_{F_{iw},V_H}, from numerical tornado simulator and those from the numerical wind tunnel is firstly conducted. The horizontal wind speed at mean eave height in tornado, V_H, and the corresponding angle of attack, θ_H, is determined in Eqs. (13) and (14)

$$V_H(r) = \sqrt{u_H^2 + v_H^2} \tag{13}$$

$$\theta_H(r) = \arctan\left(\frac{u_H}{v_H}\right) \tag{14}$$

The radial variations of V_H and θ_H in tornado are shown in Fig. 9. It is found that θ_H in the outer region is about 30° and reaches to 0° at the center of tornado.

The radial variation of the force coefficients, C_{F_{iw},V_H}, obtained from the tornado simulator is shown in Fig. 10. C_{F_{iw},V_H}, in the wind tunnel with angle of attack, θ, same as θ_H in tornado, are also plotted. It can be found that the force coefficients from the wind tunnel greatly underestimate those from the tornado simulator. The tornado-induced lateral forces are about 50% larger than those from the wind tunnel. For the vertical force, wind induced vertical forces from tornado simulator and those from wind tunnel are close, however the tornado induced strong pressure drop is the main contribution of the vertical force and makes the total vertical force be about three times as large as that from wind tunnel, which is consistent with the research by Haan et al. (2010). With the consideration that the maximum tornado-induced forces occur at the location about $r = r_{H,\,max}$ and the complication of the flow in the core region, the force coefficients on the building located in the outer region, $r \geq r_{H,\,max}$, are examined in this study.

The discussion above is based on the wind velocity at the mean eave height, V_H, however, it is meaningful to check if the tornado-induced wind fields below the building height are same as those from the wind tunnel. The wind profiles under the height of the building in the tornado-like vortex are plotted in Fig. 11. It can be found that the boundary layer is thin as shown in Fig. 11(a) and a kind of spiral could clearly be identified in Fig. 11(b), where θ shows the largest value near the surface and then decreases with increase of the height. The sketch of the profile near the ground could be conceived as shown in Fig. 12, where β shows the difference between the angle of attack at m.e.h, θ_H, and that at surface, θ_S.

In order to unify the wind profiles in tornados and those from straight-line wind, another force coefficient is proposed as

$$C_{F_{iw},V_v}(\theta_V) \equiv \frac{F_{iw}}{1/2V_v^2 A_i} \tag{15}$$

where V_v is the volume averaged wind speed and θ_v is the volume averaged angle of attack. V_v and θ_v are calculated in Eqs. (16) and (17)

$$V_v(r) = \sqrt{u_v^2 + v_v^2} \tag{16}$$

$$\theta_v(r) = \arctan\left(\frac{u_v}{v_v}\right) \tag{17}$$

in which the volume averaged velocities, u_v and v_v, are defined as

$$u_v = \frac{\oint_\Omega u d\Omega}{\Omega};\ \ v_v = \frac{\oint_\Omega v d\Omega}{\Omega} \tag{18}$$

where u and v denote velocity components in x and y directions respectively, and Ω is the volume occupied by the building model. The radial variations of V_v and θ_v in tornado are illustrated in Fig. 13, where V_H and θ_H are also plotted to show the difference. The ratio of the magnitude of volume averaged velocity to the

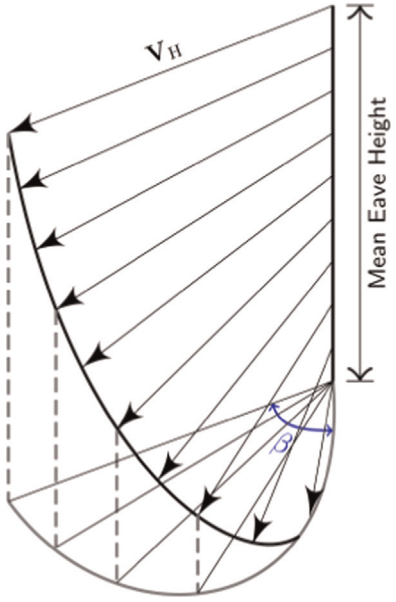

Fig. 12. Sketch of the spiral of the wind in the tornado near the ground.

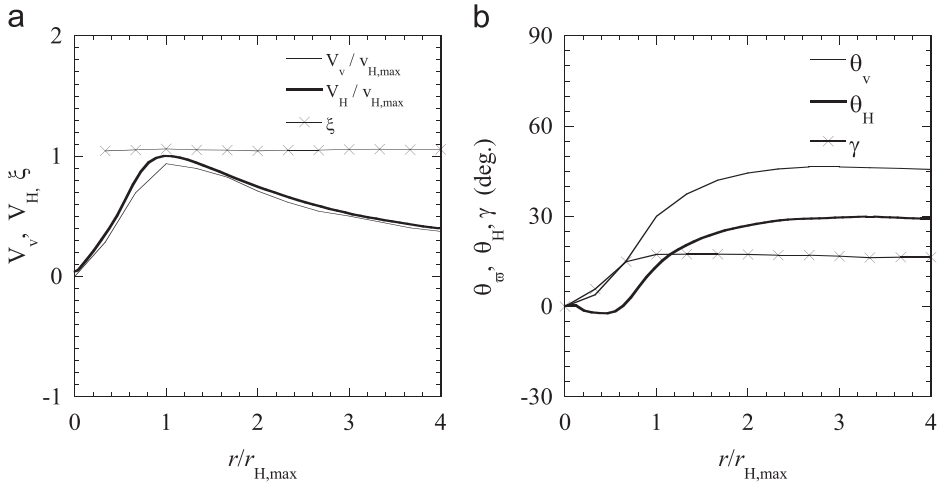

Fig. 13. Radial variation of, (a) wind speed and (b) direction of the volume averaged velocity for tornado-like vortex.

magnitude of the velocity at mean eave height, ξ, and the difference between θ_v and θ_H, γ, are expressed as

$$\xi = \frac{V_H}{V_v};\ \gamma = \theta_v - \theta_H \tag{19}$$

ξ and γ are the function of the radial distance, r, the swirl ratio, S, the ground roughness length, z_0, the translation speed of tornado, V_T, the volume occupied by the structure, Ω, and the size of the building, L. In this study we only consider a stationary F4 tornado and one certain building model, therefore S, z_0, V_T, Ω, and L are all constant. What we changed is just the radial distance, r. The plots of ξ and γ at several radial locations in the simulated tornado are also illustrated in Fig. 13. It can be found that ξ is nearly 1.0 which is due to the thin boundary layer, and γ shows nearly constant value, 17°, at $r \geq r_{H,\,max}$.

For the air flow in the wind tunnel, ξ is the function of the ground roughness length, z_0, and the volume occupied by the structure, Ω. It is calculated as 1.22 in this study. The deflection angle, γ, is 0 since there is no spiral profile in the wind tunnel.

The force coefficients, $C_{F_{iw,V_v}}$, in the tornado at several radial locations are shown in Fig. 14. $C_{F_{iw,V_v}}$, in the wind tunnel with angle of attacks, θ, same as $\theta_v(r)$ in tornado, are also plotted, which could be obtained through multiplying the data in Fig. 9 with $\xi^2 = 1.49$. It can be found that the results from wind tunnel show good agreement with those from the tornado simulator with errors in a range of 6%. For estimating the forces in the region, $0 \leq r < r_{H,\,max}$, the force coefficients, $C_{F_{iw,V_v}}$, are conveniently assumed same as those at $r = r_{H,\,max}$. From the following discussion we could find this assumption is safe and could provide reasonable results.

In a tornado-induced flow field, $F_{i,p}$ could be directly calculated by some models, such as the Rankine model, the model proposed by Kikitsu et al. (2012), and so on. In the future we want to propose a more appropriate model but in the present study we will directly use the pressure distribution obtained from the simulation, as shown in Fig. 5(b), since the target of the present study is to give an idea to link the straight-line wind induced forces and the forces due to the direct action of wind in the tornado. $F_{i,w}$ could be estimated by the force coefficients, $C_{F_{iw,V_v}}$, obtained from wind tunnel. As a result, the total forces, $F_{i,t}$, could be calculated as

$$F_{i,t} = F_{i,p} + C_{F_{iw,V_v}} \cdot 1/2\rho V_v^2 A_i \tag{20}$$

The estimated force coefficients, $C_{F_{iw,v_{H,\,max}}}$, as defined in Eq. (10) are shown in Fig. 15. It is found that the magnitudes of the force coefficients agree well with the direct simulation in the tornado simulator, indicating that the tornado induced forces can be successfully estimated using the force coefficients obtained from the wind tunnel even though the wind profiles of these two situations are different. It is needed to be pointed out that the existence of the building will definitely disturb the flow fields of the tornado. In the present study, the proposed method works due to the ratio, λ_B, of the building size, L, to the size of the tornado, $r_{H,\,max}$, is small enough which is only 1/3 and the disturbance from the building is not obvious. If λ_B is over some limitations the proposed method should be modified and one coefficient, $C_{\lambda B}$, considering λ_B should be introduced

$$F_{it} = C_{\lambda B}(\lambda_B)\left(F_{ip} + C_{F_{iw,V_V}} \cdot 1/2\rho V_V^2 A_i\right) \tag{21}$$

In order to provide further evidences to support the proposed normalization method based on V_v and θ_v, the pressure distributions on the building model located in tornado with $r = r_{H,\,max}$, where $\theta_H = 10^\circ$ and $\theta_V = 30^\circ$, and those in the straight-line wind with angles of attack equal to 10° and 30° are chosen to do discussion. The pressure contours are plotted in exploded form as shown in Fig. 16, the side walls and roof of the building model are named as Face1, Face2, Face3, Face4 and Roof, respectively. The pressure has been normalized by using $1/2\rho V_V^2$.

Fig. 16(a) shows the pressure contour on the building when it is placed in the tornado-like vortex. It is deserved to be pointed out that in the plotting the tornado-induced atmospheric pressure has been removed. It is found that on Face1 and Face2 pressure coefficients are mostly positive because of the directly blowing of wind, therefore Face1 and Face2 can be seen as windward sides. On the other hand negative pressure coefficients occupy Face3 and Face4 in which the large-scale flow separations occur, as a result they act as leeward sides. Because of the unbalanced pressure

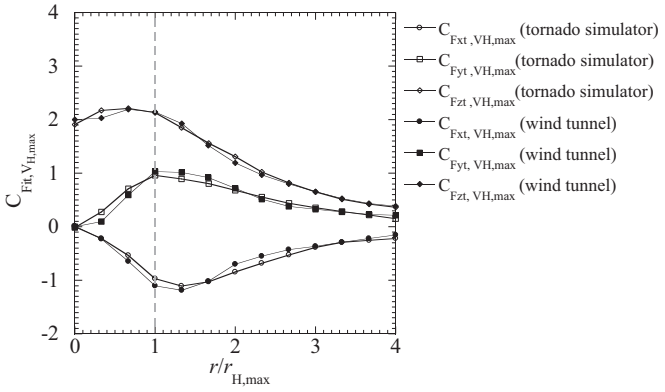

Fig. 15. Comparison of force coefficients, $C_{F_{it},v_{H,\,max}}$, between those directly calculated from the tornado simulator and those estimated from the wind tunnel.

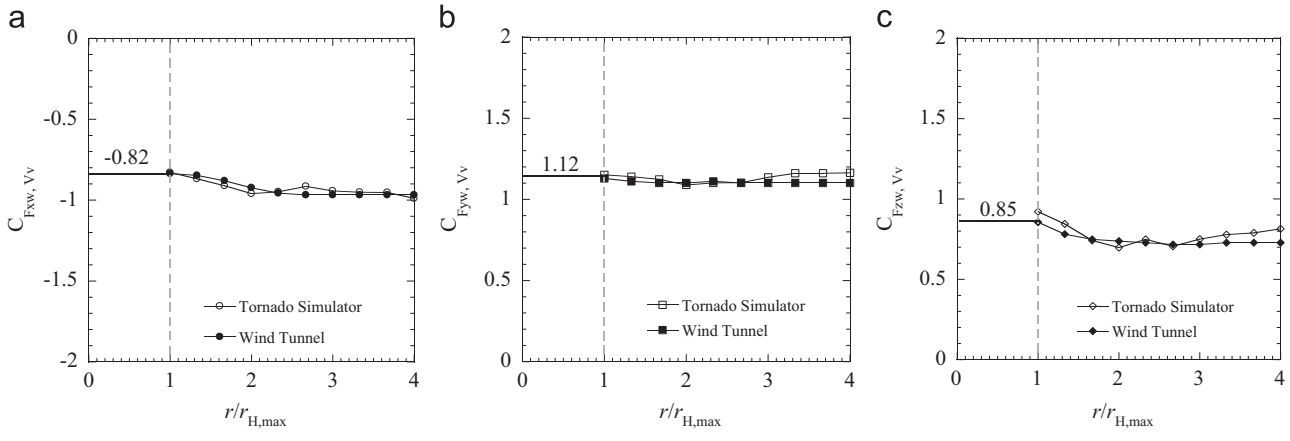

Fig. 14. Comparison of force coefficients, $C_{F_{iw,V_v}}$, from tornado simulator and those from wind tunnel, (a) radial component, (b) tangential component, and (c) vertical component.

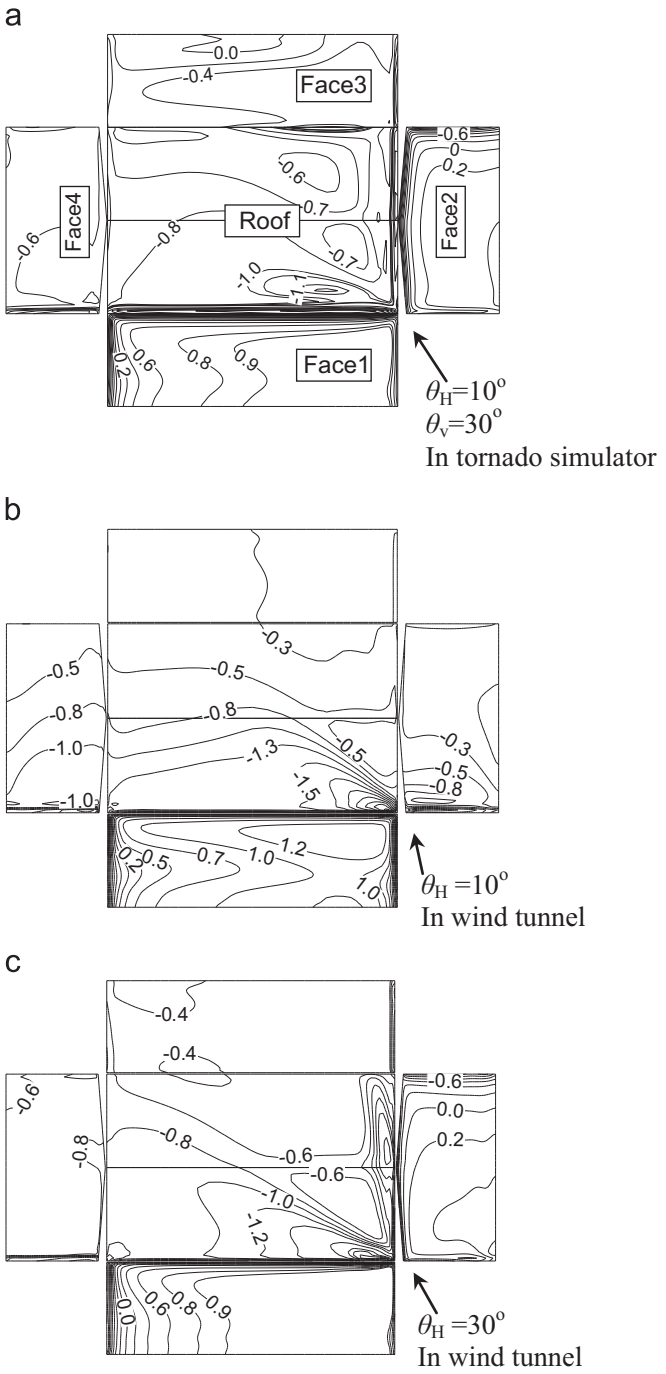

Fig. 16. Mean pressure contour on building model when located at, (a) the outer boundary of tornado core in tornado simulator with θ_H=10° and θ_v=30°, (b) in wind tunnel with angle of attack θ being 10° and (c) angle of attack θ being 30°.

distribution between Face1 and Face3 and that between Face2 and Face4, the tornado-induced aerodynamic forces tend to move the building model tangentially and closing to the center, which is consistent with the discussion in Section 3. Additionally, the pressure coefficients on the roof of the building are negative owing to the flow separation from the windward sides. As have been introduced that the tornado-induced atmospheric pressure have been removed in this plotting, the negative pressure distribution on the roof is totally due to the wind.

The pressure distributions on the building model located in the straight-line winds with angle of attack equaling to 10°, see Fig. 16 (b), and 30°, see Fig. 16(c), are plotted for comparison. It is clearly observed that when the angle of attack equals to 10° the positive pressure coefficients can only be found on Face1, which means that only Face1 withstand the direct impact of wind. After meeting Face1, the flow separates, due to which negative pressure distribution forms on the other three side walls and the roof of the building. This kind of distribution is obviously different with that induced by tornado even the wind directions at the m.e.h. are same. However, when the angle of attack equals to 30°, the pressure on Face1 and Face2 is mainly positive with reverse be true for Face3 and Face4, and the distribution of the pressure coefficient is very comparable with that in tornado.

Based on the above pressure comparison, it is further validated that volume averaged velocity is the linkage between tornado-induced forces and straight-line wind induced forces.

5. Conclusions

The forces acting on a gable-roof building induced by a tornado were investigated by the LES turbulence model. The conclusions in this study are summarized as follows: firstly, a numerical tornado simulator is generated with capability of simulating the tornado-induced forces on the building model. Predicted flow fields of the tornado-like vortex and the aerodynamic forces on the building model show good agreement with those from experiments Secondly, using the conventional force coefficients from the wind tunnel will underestimate the forces induced by the tornado with errors exceeding 50% at the outer boundary of tornado core, which results from the difference of the wind profiles. At last, one method based on volume averaged wind speed is proposed to estimate the tornado induced forces through the wind tunnel, and the results show good performance even the wind profiles of these two situations are different. The discrepancies between the results directly obtained from numerical tornado simulator and those from the straight-line numerical wind tunnel are in the acceptable range of 10%.

References

Alrasheedi N.H., Selvam R.P., 2011. Tornado forces on different building sizes using computer modeling. In: Proceedings of the ASME Early Career Technical Conference, United States.

Blocken, B., Carmeliet, J., Stathopoulos, T., 2007. CFD evaluation of wind speed conditions in passages between parallel buildings—effect of wall-function roughness modifications for the atmospheric boundary layer flow. J. Wind Eng. Ind. Aerodyn. 95, 941–962.

Church, C.R., Snow, J.T., Baker, G.L., Agee, E.M., 1979. Characteristics of tornado-like vortices as a function of swirl ratio: a laboratory investigation. J. Atmos. Sci. 36, 1755–1776.

Doswell III, C., Carbin, G., Brooks, H., 2012. The tornadoes of spring 2011 in the USA: an historical perspective. Weather 67, 88–94.

Ferziger, J., Peric, M., 2002. Computational Method for Fluid Dynamics, 3rd Edition Springer, Berlin.

Haan, F.L., Sarkar, P.P., Gallus, W.A., 2008. Design, construction and performance of a large tornado simulator for wind engineering applications. Eng. Struct. 30, 1146–1159.

Haan, F.L., Balarmudu, V.K., Sarkar, P.P., 2010. Tornado-induced wind loads on a low-rise building. J. Struct. Eng. 136, 106–116.

Hangan, H., Kim, J.-D., 2008. Swirl ratio effects on tornado vortices in relation to the Fujita scale. Wind Struct. 11, 291–302.

Hoxey, R.P., Richards, P.J., 1993. Flow patterns and pressure field around a full-scale building. J. Wind Eng. Ind. Aerodyn. 50, 203–212.

Hu, H., Yang, Z., Sarkar, P., Haan, F., 2011. Characterization of the wind loads and flow fields around a gable-roof building model in tornado-like winds. Exp. Fluids 51, 835–851.

Ishihara, T., Oh, S., Tokuyama, Y., 2011. Numerical study on flow fields of tornado-like vortices using the LES turbulence model. J. Wind Eng. Ind. Aerodyn. 99, 239–248.

Ishihara, T., Liu, Z., 2014. Numerical study on dynamics of a tornado-like vortex with touching down by using the LES turbulent model. Wind Struct. 19, 89–111.

Jischke, M.C., Light, B.D., 1983. Laboratory simulation of tornadic wind loads on a rectangular model structure. J. Wind Eng. Ind. Aerodyn. 13, 371–382.

Kikitsu H., Okuda Y., Kawai H., Kanda J., 2012. Experimental study on characteristics of tornado-induced wind force on a low-rise building. In: Proceedings of the 2012 Annual Meeting of Japan Society of Fluid Mechanics (in Japanese).
Kopp, G., Chen, Y., 2006. Database-assisted design of low-rise buildings: aerodynamic considerations for a practical interpolation scheme. J. Struct. Eng. 132, 909–917.
Lee, B.D., Wilhelmson, R.B., 1997a. The numerical simulation of non-supercell tornadogenesis. Part I, Initiation and evolution of pretornadic misocyclone circulation along a dry outflow boundary. J. Atmos. Sci. 54, 32–60.
Lee, B.D., Wilhelmson, R.B., 1997b. The numerical simulation of non-supercell tornadogenesis. Part II, Evolution of a family of tornadoes along a weak out flow boundary. J. Atmos. Sci. 54, 2387–2415.
Lewellen, D.C., Lewellen, W.S., Xia, J., 2000. The influence of a local swirl ratio on tornado intensification near the surface. J. Atmos. Sci. 57, 527–544.
Maruyama, T., 2011. Simulation of flying debris using a numerically generated tornado-like vortex. J. Wind Eng. Ind. Aerodyn. 99, 249–256.
Matsui M. and Tamura Y., 2009. Influence of swirl ratio and incident flow conditions on generation of tornado-like vortex. In: Proceedings of the EACWE 5, CD-ROM.
Mochida, A., Murakami, S., Shoji, M., Ishida, Y., 1993. Numerical simulation of flowfield around texas tech building by large eddy simulation. J. Wind Eng. Ind. Aerodyn. 46–47, 455–460.
Mishra, A.R., James, D.L., Letchford, C.W., 2008. Physical simulation of a single-celled tornado-like vortex, Part B: Wind locading on a cubical model. J. Wind Eng. Ind. Aerodyn. 96, 1258–1273.
Monji, N., 1985. A laboratory investigation of the structure of multiple vortices. J. Meteorol. Soc. Jpn. 63, 703–712.
Oka, S., Ishihara, T., 2009. Numerical study of aerodynamic characteristics of a square prism in a uniform flow. J. Wind Eng. Ind. Aerodyn. 97, 548–559.
Pierre, L.M., Kopp, G.A., Surry, D., Ho, T.C.E., 2005. The UWO contribution to the NIST aerodynamic database for wind loads on low buildings: Part 2. Comparison of data with wind load provisions. J. Wind Eng. Ind. Aerodyn. 93, 31–59.
Rajasekharan, S.G., Matsui, M., Tamura, Y., 2013a. Characteristics of internal pressures and net local roof wind forces on a building exposed to a tornado-like vortex. J. Wind Eng. Ind. Aerodyn. 112, 52–57.
Rajasekharan, S.G., Matsui, M., Tamura, Y., 2013b. Ground roughness effects on internal pressure characteristics for buildings exposed to tornado-like flow. J. Wind Eng. Ind. Aerodyn. 122, 113–117.
Refan, M., 2014. Physical Simulation of Tornado-Like Vortices.. Western University, Doctoral Dissertation.
Rotz J., Yeh G., Bertwell W., 1974. Tornado and Extreme Wind Design Criteria for Nuclear Power Plants: Topical Report, San Francisco, California.
Tamura, T., Kawai, H., Kawamoto, S., Nozawa, K., Sakamoto, S., Ohkuma, T., 1997. Numerical prediction of wind loading on buildings and structures-activities of AIJ cooperative project on CFD. J. Wind Eng. Ind. Aerodyn. 67–68, 671–685.
Tamura, T., Nozawa, K., Kondo, K., 2008. AIJ guide for numerical prediction of wind loads on buildings. J. Wind Eng. Ind. Aerodyn. 96, 1974–1984.
Tamura, Y., Kikuchi, H., Hibi, K., 2001. Extreme wind pressure distributions on low-rise building models. J. Wind Eng. Ind. Aerodyn. 89, 1635–1646.
Tari, P.H., Gurka, R., Hangan, H., 2010. Experimental investigation of tornado-like vortex dynamics with swirl ratio: the mean and turbulent flow fields. J. Wind Eng. Ind. Aerodyn. 98, 936–944.
Ward, N.B., 1972. The exploration of certain features of tornado dynamics using a laboratory model. J. Atmos. Sci. 29, 1194–1204.
Wilson, T., 1977. Tornado Structure Interaction: A Numerical Simulation, Report. California University, Lawrence Livermore Lab, Livermore, United States.
Wurman, J., Alexander, C.R., 2005. The 30 may 1998 Spencer, South Dakota, storm. Part II: Comparison of observed damage and radar-derived winds in the tornadoes. Mon. Weather Rev. 133, 97–119.
Yang, Z., Sarkar, P., Hu, H., 2010. Visualization of flow structures around a gable-roofed building model in tornado-like winds. J. Vis. 13, 285–288.
Yang, Z., Sarkar, P., Hu, H., 2011. An experimental study of a high-rise building model in tornado-like winds. J. Fuilds Struct. 27, 471–486.
Yang, W., Quan, Y., Jin, X., Tamura, Y., Gu, M., 2008. Influences of equilibrium atmosphere boundary layer and turbulence parameter on wind loads of low-rise buildings. J. Wind Eng. Ind. Aerodyn. 96, 2080–2092.